Revisiting the Sulfur-Water Chemical System in the Middle Atmosphere of Venus

Wencheng Shao, Xi Zhang, Carver Bierson, Therese Encrenaz

▶ **To cite this version:**

Wencheng Shao, Xi Zhang, Carver Bierson, Therese Encrenaz. Revisiting the Sulfur-Water Chemical System in the Middle Atmosphere of Venus. Journal of Geophysical Research. Planets, 2020, 125 (8), pp.e06195. 10.1029/2019JE006195 . hal-03250477

HAL Id: hal-03250477
https://hal.science/hal-03250477

Submitted on 11 Jun 2021

HAL is a multi-disciplinary open access archive for the deposit and dissemination of scientific research documents, whether they are published or not. The documents may come from teaching and research institutions in France or abroad, or from public or private research centers.

L'archive ouverte pluridisciplinaire **HAL**, est destinée au dépôt et à la diffusion de documents scientifiques de niveau recherche, publiés ou non, émanant des établissements d'enseignement et de recherche français ou étrangers, des laboratoires publics ou privés.

Copyright

Check for updates

JGR Planets

RESEARCH ARTICLE
10.1029/2019JE006195

Key Points:
- We found that there is no bifurcation behavior in the sulfur-water chemical system as previously claimed
- The observed SO_2-H_2O anticorrelation can be explained by the sulfur-water chemistry with mixing ratio variations at the middle cloud top
- This suggests that the observed temporal variations of SO_2 and H_2O are linked to the lower atmospheric processes

Supporting Information:
- Supporting Information S1

Correspondence to:
W. D. Shao,
wshao7@ucsc.edu

Citation:
Shao, W. D., Zhang, X., Bierson, C. J., & Encrenaz, T. (2020). Revisiting the sulfur-water chemical system in the middle atmosphere of Venus. *Journal of Geophysical Research: Planets*, *125*, e2019JE006195. https://doi.org/10.1029/2019JE006195

Received 3 SEP 2019
Accepted 6 APR 2020
Accepted article online 26 JUN 2020

©2020. American Geophysical Union. All Rights Reserved.

Revisiting the Sulfur-Water Chemical System in the Middle Atmosphere of Venus

Wencheng D. Shao[1], Xi Zhang[1], Carver J. Bierson[1], and Therese Encrenaz[2]

[1]Department of Earth and Planetary Sciences, University of California, Santa Cruz, CA, USA, [2]LESIA, Observatoire de Paris, PSL University, CNRS, Sorbonne University, University Sorbonne Paris City, Meudon, France

Abstract Sulfur-water chemistry plays an important role in the middle atmosphere of Venus. Ground-based observations have found that simultaneously observed SO_2 and H_2O at ~64 km vary with time and are temporally anticorrelated. To understand these observations, we explore the sulfur-water chemical system using a one-dimensional chemistry-diffusion model. We find that SO_2 and H_2O mixing ratios above the clouds are highly dependent on mixing ratios of the two species at the middle cloud top (58 km). The behavior of sulfur-water chemical system can be classified into three regimes, but there is no abrupt transition among these regimes. In particular, there is no bifurcation behavior as previously claimed. We also find that the SO_2 self-shielding effect causes H_2O above the clouds to respond to the middle cloud top in a nonmonotonic fashion. Through comparison with observations, we find that mixing ratio variations at the middle cloud top can explain the observed variability of SO_2 and H_2O. The sulfur-water chemistry in the middle atmosphere is responsible for the H_2O-SO_2 anticorrelation at 64 km. Eddy transport change alone cannot explain the variations of both species. These results imply that variations of species abundance in the middle atmosphere are significantly influenced by the lower atmospheric processes. Continued ground-based measurements of the coevolution of SO_2 and H_2O above the clouds and new spacecraft missions will be crucial for uncovering the complicated processes underlying the interaction among the lower atmosphere, the clouds, and the middle atmosphere of Venus.

Plain Language Summary Sulfur chemistry composes one important chemical cycle in the Venusian atmosphere. Sulfur dioxide, the most abundant sulfur species, is transported from the lower atmosphere (below the clouds) to the middle atmosphere. On the dayside, sulfur dioxide is dissociated by ultraviolet light and forms various sulfur-bearing species. These species, like polysulfur and sulfuric acid, are critical for the formation of Venus' haze and the sulfuric acid clouds. Sulfur dioxide is observed to vary by orders of magnitude, though mechanisms underlying those variations remain elusive. In this work, we use a one-dimensional photochemical model to explain the coevolution of sulfur dioxide and water from ground-based observations. We find that sulfur chemistry and variations inside the clouds are two important factors affecting temporal variations of sulfur dioxide and water. Our study highlights the importance of the interaction among the lower atmosphere, the clouds, and the middle atmosphere on Venus.

1. Introduction

The sulfur cycle is one major part of the complicated chemistry in the Venus atmosphere. (Yung & DeMore, 1982). Sulfur oxides react with water and form the sulfuric acid clouds at 60–70 km (Hansen & Hovenier, 1974; Young, 1973). Those clouds block the ultraviolet (UV) photons globally and separate the Venus atmosphere into two distinct regions in terms of tracer transport and chemistry. The lower atmosphere is characterized by thermochemistry and vigorously convective mixing. The upper part, usually termed as the middle atmosphere ranging from 60 to 100 km, is stably stratified, and photochemistry plays an important role. Previous work (e.g., Krasnopolsky, 2012, 2013, 2018; Mills, 1998; Yung & DeMore, 1982; Zhang et al., 2012) used one-dimensional (1-D) photochemistry-transport models to explain species abundances in the middle atmosphere. Those models can explain vertical profiles of species like HCL, OCS, SO_2, and SO. But not much effort has been put forth on explaining variability of those species.

The Pioneer Venus spacecraft and the International Ultraviolet Explorer observed that SO_2 mixing ratio at the cloud top (~70 km) decreases by an order of magnitude during 1970s and 1980s (Esposito, 1984; Esposito et al., 1988; Na et al., 1990). The SPICAV instrument onboard the Venus Express spacecraft

observed a secular increase in SO_2 at the cloud top between mid-2006 and 2007 (Marcq et al., 2013) and then an overall decrease from 2007 to 2014 (Marcq et al., 2013, 2019; Vandaele et al., 2017). Ground-based observations from the TEXES high-resolution imaging spectrometer at the NASA Infrared Telescope Facility (IRTF) also detected long-term variations of SO_2 at 64 km (near the cloud top) in 2012–2019 (Encrenaz et al., 2016, 2019a). The SPICAV and the TEXES data also show that SO_2 above or near the cloud top has large short-term and spatial variations (Encrenaz et al., 2012, 2013, 2016; Vandaele et al., 2017). For water, ground-based telescopes found temporal variations in the disk-integrated H_2O abundance (Encrenaz et al., 2016, 2019a; Sandor & Clancy, 2005). But TEXES discovered that H_2O at 64 km, unlike SO_2, exhibits relatively uniform spatial distribution over the Venus disk (Encrenaz et al., 2012, 2013).

Although 1-D models can explain the observed vertical profiles of SO_2 in the middle atmosphere through eddy diffusion and photochemistry (e.g., Krasnopolsky, 2012, 2013, 2018; Mills, 1998; Yung & DeMore, 1982; Zhang et al., 2012), mechanisms underlying horizontal and temporal variations of sulfur species and water are still not well understood. Proposed explanations include middle atmospheric photochemistry (e.g., Parkinson et al., 2015; Vandaele et al., 2017) and flux variations from the lower atmosphere due to either periodic volcanic injections (e.g., Esposito, 1984; Esposito et al., 1988) or atmospheric dynamical fluctuations (e.g., Cottini et al., 2012; Marcq et al., 2013). Discriminating these mechanisms requires detailed sulfur-water chemical models and detailed observations in high temporal and spatial resolutions.

Encrenaz et al. (2019b, 2020) simultaneously observed variations of SO_2 and H_2O at 64 km. These observations range from 2012 to 2019 and are made by TEXES in the spectral range around 7.4 μm. These observations show not only temporal variations of disk-integrated abundances but also a seemingly temporal anticorrelation between SO_2 and H_2O. The evidence of this anticorrelation is not very clear in Encrenaz et al. (2019), but with more data taken recently, the correlation is stronger (Encrenaz et al., 2019b, 2020). The cause for this anticorrelation is unknown. Parkinson et al. (2015) (hereafter P15) used the 1-D chemistry-diffusion model in Zhang et al. (2012) to study the sulfur-water chemical system in the middle atmosphere. It was found that the system is extremely sensitive to the middle cloud top mixing ratios of SO_2 and H_2O at 58 km. But mechanisms of this sensitivity are not well explored. Bierson and Zhang (2020) used a photochemical model describing the full atmosphere of Venus and pointed out that sulfur species abundances in the middle atmosphere are very sensitive to the vertical transport in the lower and middle clouds. The new TEXES data provide a unique opportunity to revisit the sulfur-water chemical system and understand the coevolution of SO_2 and H_2O in the Venus atmosphere in detail.

Using a 1-D chemistry-diffusion model, we explore the mechanisms underlying the anticorrelation and variations of SO_2 and H_2O from TEXES in this study. We find that the sulfur-water chemical system has three chemical regimes. We show that there is no chemical bifurcation claimed in previous studies (e.g., P15). We also point out that the SO_2 self-shielding effect plays an important role in this system. Combining our model with the TEXES data, we find that sulfur chemistry in the middle atmosphere accounts for the long-term anticorrelation of SO_2 and H_2O. Eddy mixing variations alone cannot produce the observed anticorrelation of both species. The temporal variations of SO_2 and H_2O at the observed altitude (64 km) are linked to variations of mixing ratios and fluxes at the middle cloud top (58 km). This implies that the observed variability probably originates from processes inside the clouds or from the lower atmosphere.

This paper is organized as follows. First we will introduce our model in section 2. In section 3 we show results from simulations and demarcate different chemical regimes, followed by explanations of mechanisms. In section 4, we compare our simulations with the TEXES data and explore possible mechanisms that could cause the observed variations and anticorrelation.

2. Model Description

In this study we use the JPL/Caltech Kinetics Venus model (e.g., Mills, 1998; Yung & DeMore, 1982; Zhang et al., 2012), as was used in P15. This chemical kinetics model has 51 species, 41 photodissociation reactions, and over 300 neutral reactions. The model details are described in Zhang et al. (2012). This is the same model used by P15, and following P15, we set the lower boundary at 58 km, the middle cloud top (Knollenberg & Hunten, 1980). Below this altitude the middle and lower cloud layers have low static stability, while above it, the Venus atmosphere is stably stratified (Imamura et al., 2017; Limaye et al., 2018; Tellmann et al., 2009). To

explore the parameter space of the sulfur-water chemical system, we vary lower boundary mixing ratios of two parent species—SO_2 and H_2O—that are transported upward from the middle cloud region. The range of SO_2 lower boundary mixing ratio is 1–75 ppm and that of H_2O is 1–35 ppm, covering the ranges of two species in P15. The temperature, pressure, total number density, and eddy diffusion profiles are all the same as Zhang et al. (2012) and P15.

Above 80 km, the volume mixing ratio of SO_2 has been observed to increase with height, implying a high-altitude sulfur source (e.g., Belyaev et al., 2012; Sandor et al., 2010). This source may be sulfuric acid or polysulfur species (Zhang et al., 2010, 2012). In this study we only use sulfuric acid as the upper sulfur source, same as in P15. Note that the amount of sulfuric acid in the upper atmosphere required to match the sulfur inversion does exceed the upper limits from ground-based observations (Sandor et al., 2012). But using polysulfur instead or even not including any upper sulfur source (thus no inversion above 80 km) does not alter our conclusions in this paper (see discussions in section 4.1).

The chemical model we use in this study solves the 1-D atmospheric continuity equation:

$$\frac{\partial X}{\partial t} = e^{\xi}\frac{\partial}{\partial z}\left(e^{-\xi}\,K_{zz}\,\frac{\partial X}{\partial z}\right) + \frac{P-L}{n} \tag{1}$$

(e.g., Zhang et al., 2013). Here X is the volume mixing ratio of a chemical species. $\xi = z/H$, and H is the pressure scale height of the background atmosphere. K_{zz} is the eddy diffusivity. P and L are the total production and loss rates, respectively. n is the number density of the background atmosphere. The first and second terms in the right-hand side are the eddy diffusion and net production, respectively. The molecular diffusion is ignored below the homopause, ~125 km, on Venus. When the chemical system reaches the steady state, the eddy diffusion and net production should balance each other for every species.

The chemistry-diffusion system is usually numerically stiff as the chemical reaction rates could differ by several orders of magnitude. This system can be solved using an implicit Euler time stepping scheme, allowing the time step to exponentially increase in the time marching. A traditional convergence criterion is to check the abundance differences of the chemical species in two successive time steps. If the relative difference is sufficiently small, the model is considered to have reached the steady state. This was the criterion used in P15. Using the same model setup and the traditional convergence criterion, we can reproduce the simulation results of P15 (supporting information Figures S2a–S2c). However, we found that some cases do not actually reach the steady states defined by Equation 1; that is, the eddy diffusion and net production terms do not exactly balance each other. See Text S1 and Figure S1 for an example case and discussions.

To ensure that the model simulations reach the real steady state, in this study, we reinforce a more rigorous convergence criterion, that is, eddy diffusion and net production must equal in Equation 1 for every species. See an example case in the supporting information. Under this new criterion, we reached different simulation results and conclusions from that of P15 (see Figure S2), as discussed in the following section.

3. SO_2 and H_2O Variability Above the Clouds

Following P15, Figure 1 shows SO_2, H_2O, and SO_3 mixing ratio variations (hereafter "maps") at 80 km as a function of SO_2 and H_2O mixing ratios at 58 km (the middle cloud top). Here we adopt the same parameter setting as that in P15 to make comparison. In P15's Figures 9 and 10, SO_2 and H_2O maps are "antisymmetric" across mixing ratio ranges at 58 km (also see Figures S2a and S2b in this study). P15 found two regimes, high SO_2-low H_2O and low SO_2-high H_2O. The transition between the two regimes is abrupt and is called the "chemical bifurcation." However, in our work, the SO_2 and H_2O maps (Figures 1 and S2d–S2f) do not have these behaviors. First, the SO_2 and H_2O maps are not "antisymmetric." Second, it appears no chemical bifurcation or abrupt transition. Instead, the most salient feature is the nonmonotonic behavior of H_2O variations as a function of SO_2 at 58 km (Figure 1b).

According to Figure 1, we summarize behaviors of the chemical system at 80 km within three regimes:

1. Low SO_2-low H_2O. H_2O mixing ratio decreases as SO_2 at 58 km increases. SO_2 mixing ratio decreases as H_2O at 58 km increases. This pattern is similar to that of P15 except that two species do not have very abrupt changes in this regime, that is, no "chemical bifurcation."

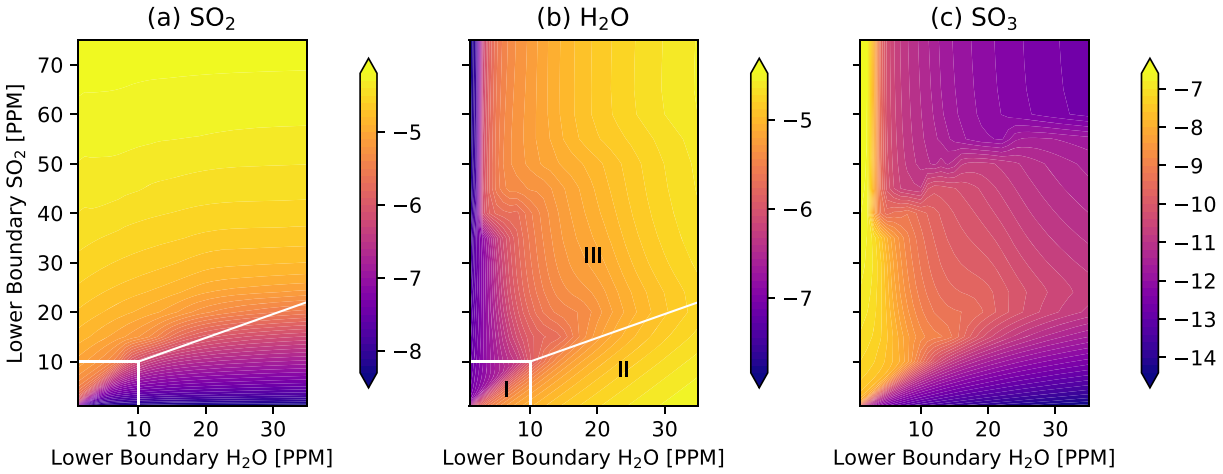

Figure 1. Mixing ratios of SO_2 (a), H_2O (b), and SO_3 (c) at 80 km as functions of SO_2 and H_2O mixing ratios at 58 km. The white lines divide species maps into three regimes, I, II, and III. Colors are volume mixing ratios on a logarithmic scale.

2. Low SO_2-high H_2O. H_2O is oversupplied. H_2O mixing ratio still decreases as SO_2 at 58 km increases. SO_2 mixing ratio remains relatively low and insensitive to changes in H_2O at 58 km. H_2O behavior is similar to that in Regime I, but SO_2 behavior is different.
3. High SO_2. H_2O mixing ratio increases as SO_2 at 58 km increases. SO_2 mixing ratio decreases as H_2O at 58 km increases. SO_2 behavior is similar to that in Regime I, but H_2O behavior is different from that in Regime I.

In all three regimes, the mixing ratio of an individual species at 80 km increases as its own mixing ratio at 58 km increases. This is primarily a result of eddy diffusive transport from the lower boundary. We also found that SO_3 and H_2O maps (Figures 1b and 1c) exhibit an anticorrelated pattern. This is due to sulfuric acid formation:

$$SO_3 + 2H_2O \rightarrow H_2SO_4 + H_2O. \quad \text{(R1)}$$

This reaction is the main chemical sink for both SO_3 and H_2O near and inside the clouds. This reaction says that two species consume each other, and increase of one species can cause decrease of the other.

Figure 1b shows that H_2O responds nonmonotonically to changes in SO_2 at 58 km. From Regime I or II to Regime III, H_2O at 80 km first decreases and then increases as SO_2 at 58 km increases. This behavior is due to the SO_2 self-shielding effect. SO_3 and H_2O consume each other via Reaction R1. In all regimes, when SO_3 above the clouds decreases, H_2O above the clouds increases. SO_3 above the clouds is mainly produced by SO_2 oxidation:

$$O + SO_2 + M \rightarrow SO_3 + M, \quad \text{(R2)}$$

where M is the background atmosphere. Reaction R2 suggests that SO_3 production is affected by abundances of both atomic oxygen O and SO_2. The atomic oxygen O above the clouds is mainly produced by SO_2 photolysis:

$$SO_2 + hv \rightarrow SO + O. \quad \text{(R3)}$$

Reaction R3 suggests that atomic oxygen production is affected by SO_2 abundance and the amount of photons (or UV light intensity).

When SO_2 at the middle cloud top increases, SO_2 above the clouds increases. This increase produces more atomic oxygen via SO_2 photolysis (R3). SO_2 oxidation (R2) then increases SO_3 production due to increase of both SO_2 and atomic oxygen. Increased SO_3 consumes more H_2O. This is the chemistry in Regimes I

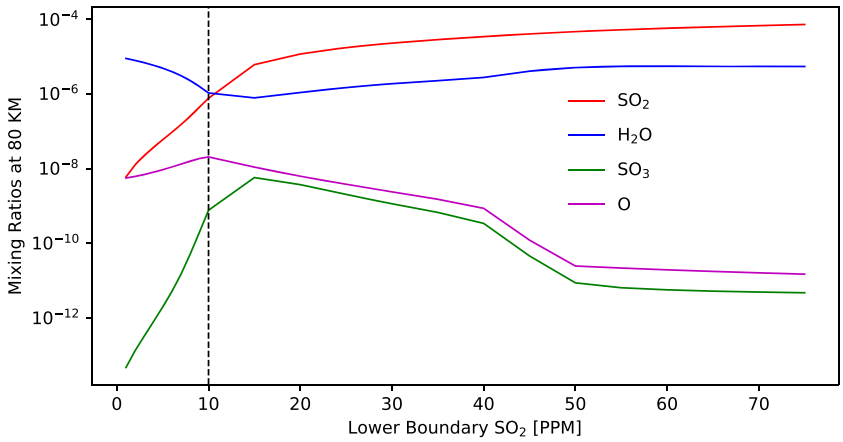

Figure 2. SO_2, H_2O, SO_3, and atomic oxygen mixing ratios at 80 km vary with SO_2 mixing ratio at 58 km. H_2O mixing ratio at 58 km is fixed as 10 ppm. The black dashed line delimits Regime I and Regime III.

and II. Figure 2 shows an example with H_2O mixing ratio fixed as 10 ppm at 58 km. When SO_2 at 58 km increases from 1 to 10 ppm, at 80 km, SO_2, atomic oxygen and SO_3 all increase while H_2O decreases.

As SO_2 inside the clouds continues increasing, SO_2 at higher altitudes becomes abundant due to eddy transport. Abundant SO_2 absorbs many photons, and thus, less photons reach lower altitudes such as 80 km. This limits atomic oxygen production via SO_2 photolysis (R3). Less atomic oxygen is produced, and this decreases SO_3 production via SO_2 oxidation (R2). Then sulfuric acid formation (R1) consumes less H_2O and H_2O is accumulated. In this process SO_2 absorption and photolysis at higher altitudes "shield" SO_2 photolysis at lower altitudes. This is the SO_2 self-shielding effect. This effect causes H_2O behaviors in Regime III. See the example in Figure 2 where H_2O at 58 km is fixed as 10 ppm. When SO_2 at 58 km increases from 10 to 50 ppm, at 80 km, SO_2 increases, atomic oxygen and SO_3 both decrease due to the SO_2 self-shielding, and consequently, H_2O increases.

SO_2 mixing ratio at 80 km generally decreases as H_2O at 58 km increases (Figure 1a). This behavior is strong in Regime I, weaker in Regime III, and almost negligible in Regime II. Our analysis suggests that some SO_3-involved reactions are key for this behavior. These reactions convert SO_3 to SO_2 and are here called SO_3 pathways:

$$SO_3 + hv \rightarrow SO_2 + O, \quad \text{(R4)}$$

$$O + SO_3 \rightarrow SO_2 + O_2, \quad \text{(R5)}$$

$$S + SO_3 \rightarrow SO_2 + SO, \quad \text{(R6)}$$

$$S_2 + SO_3 \rightarrow S_2O + SO_2, \quad \text{(R7)}$$

$$SO + SO_3 \rightarrow 2SO_2. \quad \text{(R8)}$$

To investigate the role of these SO_3 pathways, we do a test in which we shut off all pathways (R4–R8) and see how the chemical system behaves. In our test cases, SO_2 lower boundary mixing ratios are all 9 ppm. We designed two groups with (control) and without (experimental) the SO_3 pathways, respectively.

Figure 3 shows mixing ratio variations at 80 km in two groups. In the control group, SO_2 at 80 km decreases when H_2O at 58 km increases from 1 to 10 ppm. This is because more H_2O consumes more SO_3 and causes less SO_2 produced via the SO_3 pathways. When SO_3 pathways are not included (the experimental), SO_2 mixing ratio is not affected. Consequently SO_2 at 80 km remains low and insensitive to variations when H_2O at 58 km increases from 1 to 35 ppm.

When H_2O mixing ratio at 58 km is above 10 ppm, H_2O is oversupplied. In this situation, SO_3 mixing ratio is low due to efficient sulfuric acid formation, and SO_3 pathways (R4–R8) contribute little to the SO_2

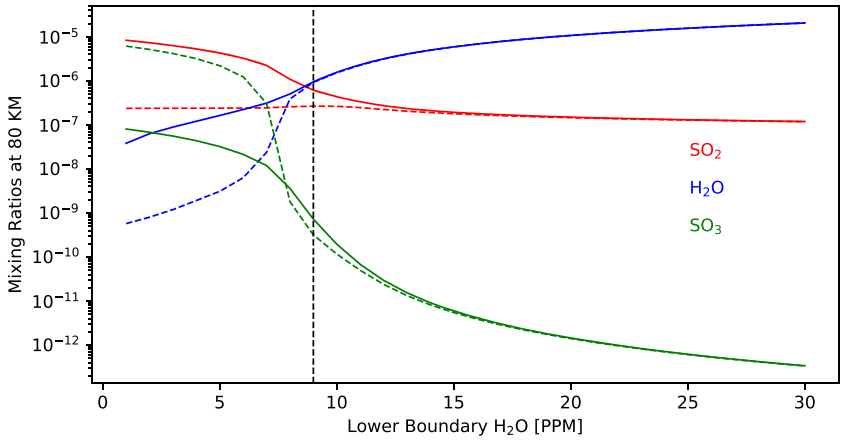

Figure 3. The mixing ratios of SO_2 (red), H_2O (blue), and SO_3 (green) at 80 km for two groups vary with H_2O mixing ratio at 58 km. SO_2 mixing ratio at 58 km is fixed as 9 ppm. In the control group (solid lines) reactions (R4–R8) convert SO_3 to SO_2, while in the experiment group (dashed lines), these reactions are shut off. The black dashed line delimits Regimes I and II.

production. As a result, SO_2 at 80 km in both the control and experimental groups remain low and insensitive to H_2O variations at 58 km. This explains the SO_2 behavior in Regime II.

4. Comparison With the TEXES Data

Encrenaz et al. (2019b, 2020) reported an anticorrelation of disk-averaged abundances of simultaneously observed SO_2 and H_2O at ~64 ± 2 km (near the upper cloud top) in 2012–2019 from TEXES/IRTF. As shown in Figures S5a and 6a, these data provide unique information about how the two parent chemical species vary together in the middle atmosphere. In particular, the apparent anticorrelation between the disk-averaged SO_2 and H_2O could be used to distinguish different proposed mechanisms for the long-term variation. Using our simple 1-D chemistry-diffusion model, here we specifically explore two possibilities. First, if the temporal variation of SO_2 and H_2O is a result of perturbations below the middle cloud top (e.g., Esposito, 1984; Esposito et al., 1988), varying the lower boundary conditions in our model should be able to reproduce the anticorrelation. On the other hand, if the variation is due to changes in the vertical mixing inside the upper cloud (e.g., Lefevre et al., 2018, 2020), changing the eddy diffusivity in our model should be able to explain the data.

To compare our model with these disk-averaged observations, we set the latitude at 45°N and assume that the SO_2-H_2O chemical system is in steady state at each individual observational time. The Venus atmosphere is highly variable on timescales of hours and days (e.g., Encrenaz et al., 2013). To isolate longer-period variations (which are more comparable to steady state simulations) we spatially average over the entire disk and temporally average over observations taken within 2 months. The chemical lifetimes of SO_2 and H_2O at 64 km are generally less than 2 months.

4.1. Middle Cloud Top Variations

To test whether the variations of SO_2 and H_2O come from the lower atmospheric processes, we first perform simulations by varying SO_2 and H_2O mixing ratios at the middle cloud top (58 km) but fixing the eddy diffusivity. We analyze SO_2, H_2O, and SO_3 variations at 64 km to explore the parameter space (Figure 4). There are also three chemical regimes at 64 km, similar to that in Figure 1 where we showed the same species at 80 km. For example, in Regime I at both altitudes, SO_2 decreases as H_2O at 58 km increases, and H_2O decreases as SO_2 at 58 km increases. But the regime boundaries are different between Figures 1 and 4. Regime I in Figure 4 only covers H_2O and SO_2 at 58 km from 0–2.6 ppm, while Regime I in Figure 1 covers both species at 58 km from 0–10 ppm.

For each individual observational data point of SO_2 and H_2O at 64 km, we fix the eddy mixing and carefully tune the SO_2 and H_2O mixing ratios at the lower boundary of our model to match the disk-averaged TEXES

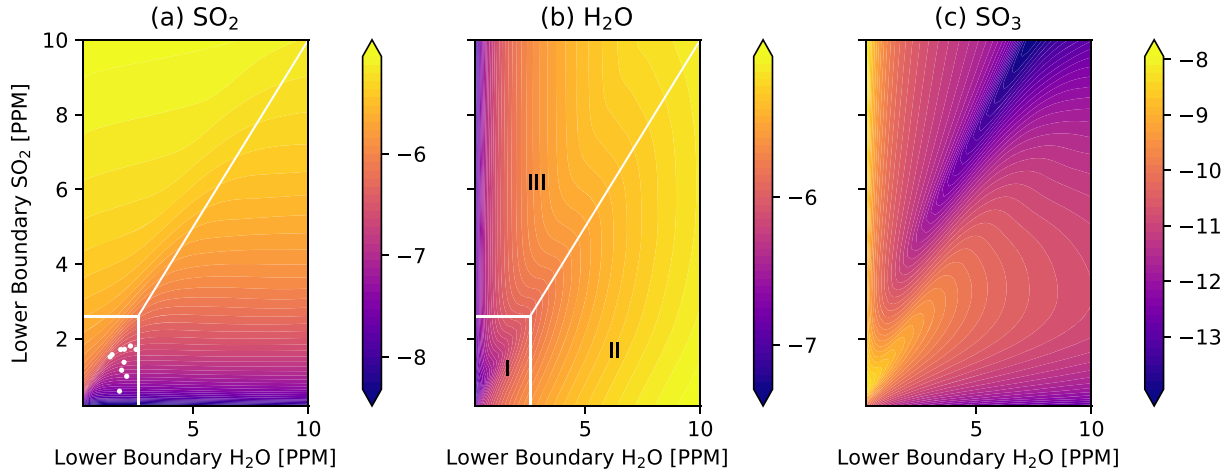

Figure 4. Same as Figure 1, but at 64 km and 45°N. White dots are models that match the TEXES observations.

observations. Figure 5 shows our simulated SO_2 and H_2O mixing ratio profiles. As altitude increases, SO_2 decreases by orders of magnitude below 80 km. H_2O remains relatively constant within a factor of 2. These structures are consistent with measurements from SOIR onboard Venus Express (e.g., Belyaev et al., 2012; Bertaux et al., 2007). From 2012 to 2019, SO_2 mixing ratio below 80 km varies in a similar way to SO_2 at 64 km, consistent with the correlated observations from TEXES and SPICAV (Encrenaz et al., 2019a). H_2O below 80 km also follows the same variation pattern as that at 64 km. In the region between 60 and 80 km, the primary sink for both SO_2 and H_2O is sulfuric acid formation (R1). Above 90 km both H_2O and SO_2 mixing ratios are supplied by our prescribed sulfur acid source. Note that removing this prescribed source hardly changes SO_2 and H_2O profiles below 70 km (Figure 5). There is some difference at 80 km between cases with and without the source, but this difference does not change three regimes discussed in section 3 except that the transitions among regimes could shift. In this section the mainly focused altitude region is below 70 km; the existence of this source is not important to our results.

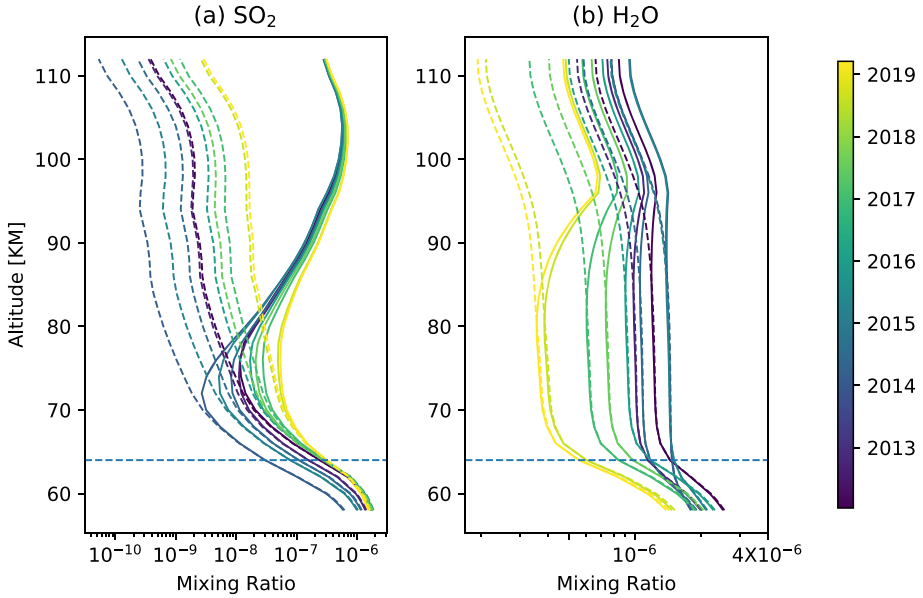

Figure 5. Simulated vertical profiles of SO_2 (a) and H_2O (b) mixing ratios consistent with the TEXES data at 64 km (horizontal dashed lines). Curves are colored by the observational dates. Solid curves are of cases with the prescribed upper source (sulfuric acid), and dashed curves are of cases without this source (i.e., no sulfuric acid photolysis).

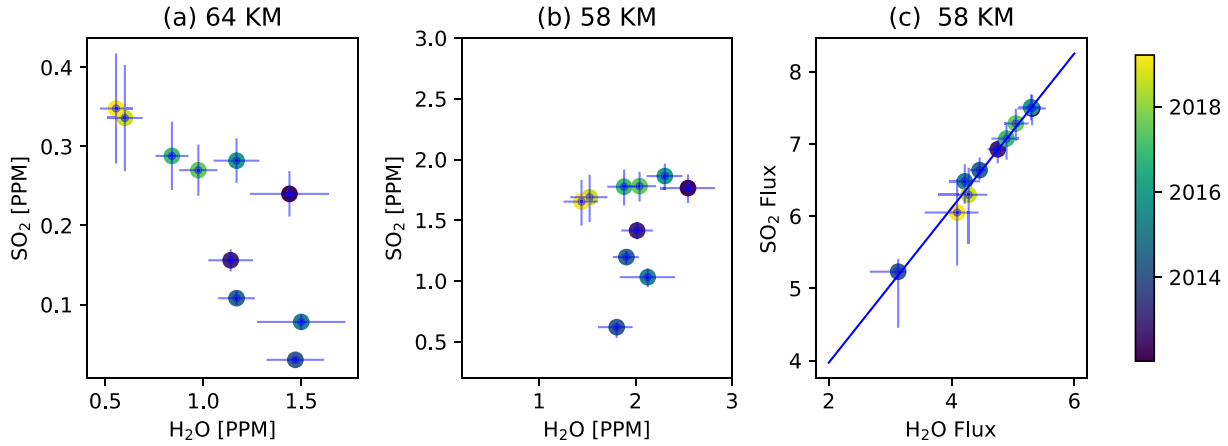

Figure 6. Scatterplots of (a) the observed SO_2 and H_2O mixing ratios at 64 km, (b) inferred mixing ratios at 58 km, and (c) upward fluxes at 58 km. Points are colored by the observational dates. The two fluxes (not considering error bars) can be fit (with1-sigma error) by $y = (1.10 \pm 0.06)x + (1.61 \pm 0.25)$, where y and x are the SO_2 and H_2O fluxes, respectively. Units of x, y, and the intercept are 10^{11} cm^{-2} s^{-1}. This fit is shown by the solid line in (c). The SO_2 and H_2O fluxes are also correlated in this manner in all of our model simulations, not just those shown.

Constrained by the TEXES data, the derived SO_2 and H_2O mixing ratios at 58 km are shown in Figure 6, along with the upward fluxes of two species at 58 km. Mixing ratio variations at 64 km can be divided into two periods: 2012–2015 and 2015–2019 (Figure 6a; Encrenaz et al., 2019a). In 2012–2015 SO_2 at 64 km varies significantly, by a factor up to 5. H_2O varies gently by a factor up to 1.5. In 2015–2019, H_2O varies by a factor over 2, and SO_2 remains relatively constant. The two different periods at 64 km also exist at 58 km (Figure 6b). This similarity between 58 and 64 km suggests that eddy diffusion plays an important role in the system in addition to photochemistry below 80 km (e.g., Jessup et al., 2015).

The fluxes of two species at 58 km show similar temporal variations to mixing ratios at 64 km (see Figures S5a and S5c). More interestingly, the two fluxes are strongly and positively correlated (Figure 6c), and the correlation coefficient is 0.99. This linear relationship feature for fluxes of two species is a result of the middle-atmosphere photochemistry in our model. Sulfuric acid formation (R1) is the major sink for SO_2 and H_2O in the middle atmosphere. If there are no other sinks, then by mass conservation, the two fluxes have to both equal the sulfuric acid formation rate. In fact because some SO_2 is also lost to the formation of the polysulfur haze, the SO_2 flux is larger than the H_2O flux (Figure 6c).

4.2. Origin of the Anticorrelation

The TEXES data show that SO_2 and H_2O at 64 km are anticorrelated (Figure 6a). The correlation coefficient is −0.80, and the linear regression slope is −0.27. But the inferred SO_2 and H_2O at the middle cloud top (58 km) do not show a good linear correlation (Figure 6b), implying that the anticorrelation behavior is not universal at all altitudes. This prediction can be tested in future observations. More importantly, the lack of a strong correlation between the two species at 58 km suggests that, although the variations of SO_2 and H_2O at 64 km might come from the lower atmospheric processes, the anticorrelation between the two species has a different mechanism.

To diagnose the system, we first notice that the TEXES observations are well located in Regime I, that is, low SO_2-low H_2O (Figure 4a). In this regime, the SO_2 self-shielding effect is insignificant. SO_2 and H_2O are linked by SO_3 via SO_2 oxidation (R2), sulfuric acid formation (R1), and SO_3 pathways (R4–R8). More SO_2 produces more SO_3 that consumes more H_2O. More H_2O consumes more SO_3 that results in less SO_2. It looks that the anticorrelation of SO_2 and H_2O might just be a characteristic of Regime I chemistry.

To test this idea, we do a statistical correlation analysis. First we run a suite of model cases in Regime I, and among these cases, both SO_2 and H_2O at 58 km are evenly spaced by 0.2 ppm between 0.2 and 2.6 ppm. Since we have 10 observations, we randomly choose 10 cases and calculate the correlation coefficient and the linear slope of SO_2 and H_2O at 64 km. We repeat the above analysis for 10,000 times and obtain the distribution of correlation coefficients and slopes (Figures 7b and 7c); 97.7% of correlation coefficients and slopes are

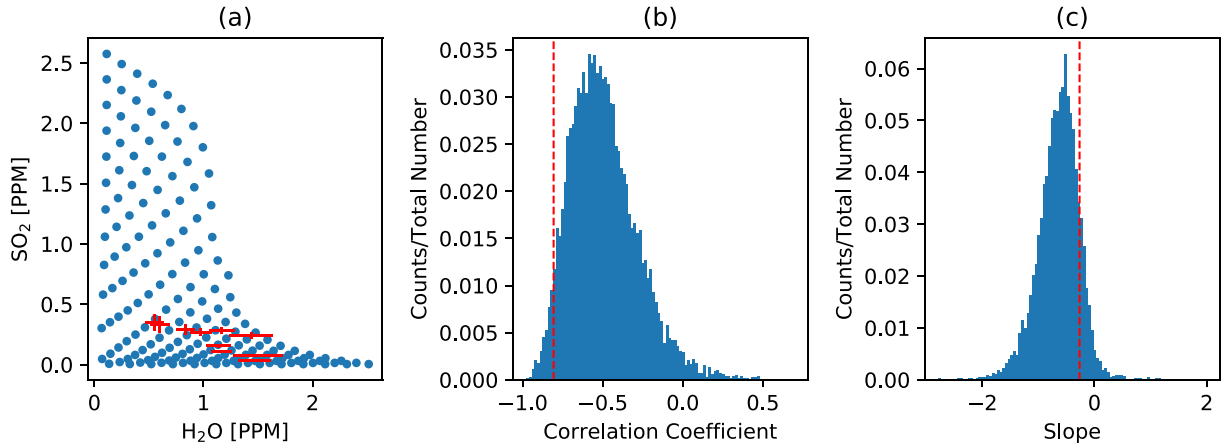

Figure 7. (a) Scatterplot of the SO_2 and H_2O mixing ratios at 64 km for all cases in Regime I (Figure 4). Red crosses are the TEXES data with error bars. (b) Statistics of 10-case correlation coefficients and (c) linear regression slopes of SO_2 and H_2O at 64 km from our model. In total we have 10,000 correlation coefficients and slopes. We use 100 bins to plot the statistical distributions. The red dashed lines are the values calculated from the TEXES data.

negative, qualitatively consistent with the sensitivity test in Krasnopolsky (2018). The correlation coefficient peaks at −0.5, and the slope peaks at −0.8. This analysis shows that if H_2O and SO_2 vary uniformly and independently at the middle cloud top, a negative correlation of SO_2 and H_2O at 64 km would be expected due to Regime I chemistry. This suggests that sulfur chemistry in Regime I together with the lower boundary variations can produce the anticorrelation of SO_2 and H_2O at 64 km.

Figure 7 shows that the observed correlation of SO_2 and H_2O differs somewhat from the model's prediction. The observed value does not locate at the center of the distributions. Although there are uncertainties in the observations, this discrepancy could also suggest that there are some second-order processes involved. It is likely that the mixing ratios of SO_2 and H_2O at 58 km do not follow a uniform distribution as assumed and may be somewhat correlated through atmospheric dynamics inside the middle clouds. Also, the exact location of the center of the distribution might depend on the choice of the eddy mixing profile in the model. But note that changing the eddy mixing alone would not produce the anticorrelation, as detailed below in section 4.3. Future observations, both remote and in situ, could help distinguish influences from these factors.

4.3. Eddy Mixing Change

Now we test whether the middle atmospheric dynamics can produce the variations and anticorrelation of SO_2 and H_2O at 64 km. In the above cases we varied the lower boundary conditions and fixed the eddy diffusivity profile (nominal, Figure 8a). The diffusivity profile is from Zhang et al. (2012), calculated based on measurements from Pioneer Venus (Von Zahn et al., 1979) and radio signal scintillations (Woo & Ishimaru, 1981). Here we fix the lower boundary conditions at 58 km but multiply this diffusivity profile by a constant factor ranging from 0.1 to 4, to explore the influence of the eddy mixing change on species mixing ratio variations at 64 km. We perform two sets of lower boundary conditions. In one set we use 1.0 ppm SO_2 and 1.0 ppm H_2O at 58 km. In the other one we use 1.7 ppm SO_2 and 2.5 ppm H_2O at 58 km. The results are shown in Figure 8b. Varying eddy mixing alone above 58 km does change the mixing ratios of SO_2 and H_2O at 64 km, but our simulations show that SO_2 is far more sensitive to the eddy mixing changes than H_2O. This difference in sensitivity of SO_2 and H_2O to eddy mixing is qualitatively consistent with Krasnopolsky (2018) and may explain the greater variations of SO_2 than H_2O over both space and time observed by TEXES (e.g., Encrenaz et al., 2013) and SPICAV (e.g., Vandaele et al., 2017). When we fix the lower boundary condition and vary the eddy mixing so that SO_2 at 64 km changes from 0 to 0.3 ppm, which is approximately the range of the observed SO_2 variations, H_2O only varies by less than 30%. In contrast, the observed abundance of H_2O has larger variations up to a factor of ~3. Also, when diffusivity increases in a large range from 0.1 to 4 times the nominal values, both SO_2 and H_2O at 64 km generally increase. Thus, we conclude that even though the eddy mixing could vary with time above 58 km, the variations of eddy

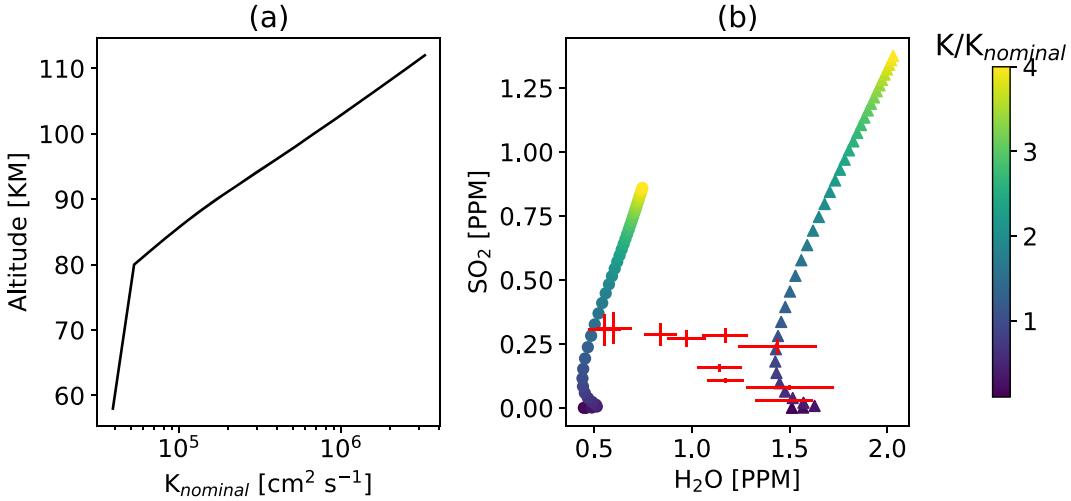

Figure 8. (a) The nominal eddy diffusivity profile in our model. (b) Scatterplot of SO_2 and H_2O mixing ratios at 64 km for various eddy diffusivity profiles. Diffusivity profiles vary from 0.1 to 4 times the nominal profile, as shown by colors. Circular markers are of cases with 1.0 ppm SO_2 and 1.0 ppm H_2O at the lower boundary. Triangular markers are of cases with 1.7 ppm SO_2 and 2.5 ppm H_2O at the lower boundary. Red crosses are the TEXES data with error bars.

mixing alone cannot explain the observed variation range of H_2O and the anticorrelation between SO_2 and H_2O at 64 km.

5. Conclusions and Discussions

In this work we revisited the sulfur-water chemical system in the middle atmosphere of Venus, motivated by the recently and simultaneously observed SO_2 and H_2O variations at ~64 km from TEXES/IRTF (Encrenaz et al., 2019b, 2020). Using a 1-D chemistry-diffusion model, we studied the coevolution of SO_2 and H_2O in the middle atmosphere of Venus for the first time. We first explored the variability of the chemical species in the system and the underlying mechanisms in a thorough way. We reported chemical regimes and mechanisms different from previous studies. Then we used our model to investigate the long-term anticorrelation of SO_2 and H_2O observed by TEXES. We tested two possible mechanisms for the anticorrelation and provided implications of those TEXES observations.

The chemical system is highly dependent on SO_2 and H_2O mixing ratios at the middle cloud top at 58 km. SO_2 and H_2O mixing ratios above the clouds vary with mixing ratios at 58 km in three regimes: low SO_2-low H_2O (Regime I), low SO_2-high H_2O (Regime II), and high SO_2 (Regime III). The pattern of Regime I is similar to that in P15 but in a much smaller parameter space. There is no chemical bifurcation or abrupt transition in Regime I. In Regime II SO_2 mixing ratio above the clouds remains low and constant as H_2O at 58 km increases. In Regime III, H_2O above the clouds increases as SO_2 at 58 km increases, different from H_2O behavior in Regime I or II. Across the regimes, there is the nonmonotonic variability of H_2O with respect to SO_2 variations at 58 km. H_2O and SO_3 variations above the clouds are antisymmetric for all three regimes due to sulfuric acid formation.

The SO_3-involved chemistry network connects SO_2 mixing ratio above the clouds to H_2O at 58 km. The nonmonotonic behavior of H_2O above the clouds results from the interplay among eddy diffusion, neutral chemistry, and photolysis processes. In those processes, the SO_2 self-shielding effect plays a crucial role.

We explored the mechanisms underlying the variations and anticorrelation between SO_2 and H_2O at 64 km from TEXES. We tested two possibilities: eddy mixing change in the middle atmosphere and species variations at the middle cloud top. Both possibilities can originate from lower atmospheric processes. We found that the eddy mixing change alone cannot produce the observed variation range of H_2O or the anticorrelation, while variations of mixing ratios at the middle cloud top with Regime I sulfur chemistry can explain both variations and the long-term anticorrelation of SO_2 and H_2O. This suggests that the observed SO_2

and H_2O variations are more likely due to perturbations on mixing ratios at the middle cloud top rather than changes in the vertical mixing alone.

Although our 1-D model provided the first and simplest explanation of the observed anticorrelation behavior of SO_2 and H_2O, our model is relatively simple with some caveats and could be improved in the future. First, our model does not include phase changes of H_2O and H_2SO_4 that could affect trace species abundances in the middle atmosphere (e.g., Gao et al., 2014; Krasnopolsky, 2015). Second, our model does not include the coupling between the lower and middle atmosphere (e.g., Bierson & Zhang, 2020), which can directly link the lower atmospheric processes to the middle atmosphere. Third, our model does not include the local time and spatial variability across latitude and longitude (e.g., Marcq et al., 2019). It would be important to revisit our proposed mechanism in a more realistic model in the future.

We also noticed discrepancies between different methods and observations of SO_2 and H_2O in the middle atmosphere. Several methods have been used to infer the water vapor abundance in the mesosphere of Venus. From Venera 15 data at 30 μm, Ignatiev et al. (1999) derived a H_2O volume mixing ratio of 10 ± 2.5 ppm at 62.5 ± 1.3 km for latitudes below 50°. Using ground-based spectroscopy at 3.3 μm, Krasnopolsky et al. (2013) inferred a H_2O mixing ratio of 3.2 ± 0.4 ppm at 74 km for latitudes below 55°. Using VIRTIS abroad Venus Express at 2.6 μm, Cottini et al. (2015) derived 3 ± 1 ppm for H_2O at 69 ± 1 km; Fedorova et al. (2016), using SPICAV at 1.38 μm, inferred $H_2O = 6$ ppm at 62 km; in both cases, low and middle latitudes were observed, and no evidence was found for local time or interannual variations. These results are all globally higher than the values inferred by TEXES. A possible reason is the choice of the D/H ratio in the Venus atmosphere. For the TEXES observations, the D/H ratio is taken equal to 200 times the Vienna Standard Ocean Water (VSMOW), following Krasnopolsky (2010), but there is some uncertainty about this parameter. Another reason might be the use of different line transitions and some uncertainty in the line parameters. Finally, in the case of TEXES, the altitude of the penetration level is not precisely defined, since the spectroscopic analysis gives information on the pressure above the continuum level and not the altitude. Nevertheless, it can be seen that all observers agree on the absence of strong local and temporal variations of H_2O at the cloud top of Venus. Indeed, between 2012 and 2016, the H_2O volume mixing ratio inferred by TEXES was more or less constant (Encrenaz et al., 2016), as pointed out by the other teams for the same period.

The main advantage of the method used with TEXES is the fact that both the SO_2 and H_2O volume mixing ratios are inferred simultaneously in location and time, at the same penetration level, from the same spectra and the same maps. Thus, the study of their local and temporal variations should not be significantly affected by uncertainty regarding the exact altitude of the penetration level. To our knowledge, TEXES is the only facility that offers this opportunity.

The continued observations of Venus using the TEXES/IRTF instrument will provide us with more information about atmospheric dynamics and tracer transport on Venus. However, due to the limited information in the cloud region and the lower atmosphere, it is still unclear that how dynamics and chemistry in the lower atmosphere, inside the clouds, and in the middle atmosphere are coupled and interacted. Besides, the decadal variations of SO_2 at the cloud top are observed since 1980s (Esposito, 1984; Esposito et al., 1988; Marcq et al., 2013; Marcq, Baggio, et al., 2019; Na et al., 1990). The underlying mechanism is elusive, although our work highlights the importance of the lower atmospheric processes. It would be crucial to continue simultaneously monitoring SO_2 and H_2O (as well as other species) in the middle and lower atmosphere, through both ground-based instruments and future spacecraft missions, to provide more clues. A three-dimensional model describing the entire Venus atmosphere involving multiple processes is expected to provide more insights into these problems in the future.

Acknowledgments

We thank Chris Parkinson, Peter Gao, Yuk Yung, and Frank Mills for their useful discussions. This work is supported by the China Scholarship Council Fellowship to W. D. S. and National Science Foundation (NSF) Grant AST1740921 to X. Z. C. J. B. was supported by the NSF Graduate Research Fellowship under Grant NSF DGE 1339067.

Data Availability Statement

Simulation data from our work are available online (https://doi.org/10.6084/m9.figshare.9696476).

References

Belyaev, D. A., Montmessin, F., Bertaux, J.-L., Mahieux, A., Fedorova, A. A., Korablev, O. I., et al. (2012). Vertical profiling of SO_2 and SO above Venus' clouds by SPICAV/SOIR solar occultations. *Icarus*, *217*(2), 740–751. https://doi.org/10.1016/j.icarus.2011.09.025

Bertaux, J.-L., Vandaele, A.-C., Korablev, O., Villard, E., Fedorova, A., Fussen, D., et al. (2007). A warm layer in Venus' cryosphere and high-altitude measurements of HF, HCl, H_2O and HDO. *Nature*, *450*(7170), 646–649. https://doi.org/10.1038/nature05974

Bierson, C. J., & Zhang, X. (2020). Chemical cycling in the venusian atmosphere: A full photochemical model from the surface to 110 km. *Journal of Geophysical Research: Planets*, *125*, e2019JE006159. https://doi.org/10.1029/2019JE006159

Cottini, V., Ignatiev, N. I., Piccioni, G., & Drossart, P. (2015). Water vapor near Venus cloud tops from VIRTIS-H/Venus Express observations 2006–2011. *Planetary and Space Science*, *113*, 219–225. https://doi.org/10.1016/j.pss.2015.03.012

Cottini, V., Ignatiev, N. I., Piccioni, G., Drossart, P., Grassi, D., & Markiewicz, W. J. (2012). Water vapor near the cloud tops of Venus from Venus Express/VIRTIS dayside data. *Icarus*, *217*(2), 561–569. https://doi.org/10.1016/j.icarus.2011.06.018

Encrenaz, T., Greathouse, T. K., Marcq, E., Sagawa, H., Widemann, T., Bézard, B., et al. (2020). HDO and SO_2 thermal mapping on Venus. V. Evidence for a long-term anti-correlation. *Astronomy & Astrophysics*. https://doi.org/10.1051/0004-6361/202037741

Encrenaz, T., Greathouse, T. K., Marcq, E., Sagawa, H., Widemann, T., Bézard, B., et al. (2019a). HDO and SO_2 thermal mapping on Venus. IV. Statistical analysis of the SO_2 plumes. *Astronomy & Astrophysics*, *623*, A70. https://doi.org/10.1051/0004-6361/201833511

Encrenaz, T., Greathouse, T., Marcq, E., Sagawa, H., Widemann, T., Bézard, B., et al. (2019b). Ground-based mapping of SO_2 and HDO on Venus in the thermal infrared. EPSC-DPS joint meeting, Sep 2019, Genève, Switzerland. EPSC-DPS2019-83. hal-02323313

Encrenaz, T., Greathouse, T. K., Richter, M. J., DeWitt, C., Widemann, T., Bézard, B., et al. (2016). HDO and SO_2 thermal mapping on Venus. III. Short-term and long-term variations between 2012 and 2016. *Astronomy & Astrophysics*, *595*, A74. https://doi.org/10.1051/0004-6361/201628999

Encrenaz, T., Greathouse, T. K., Richter, M. J., Lacy, J., Widemann, T., Bézard, B., et al. (2013). HDO and SO_2 thermal mapping on Venus. II. The SO_2 spatial distribution above and within the clouds. *Astronomy & Astrophysics*, *559*, A65. https://doi.org/10.1051/0004-6361/201322264

Encrenaz, T., Greathouse, T. K., Roe, H., Richter, M., Lacy, J., Bézard, B., et al. (2012). HDO and SO_2 thermal mapping on Venus: Evidence for strong SO_2 variability. *Astronomy & Astrophysics*, *543*, A153. https://doi.org/10.1051/0004-6361/201219419

Esposito, L. W. (1984). Sulfur dioxide: Episodic injection shows evidence for active Venus volcanism. *Science*, *223*(4640), 1072–1074. https://doi.org/10.1126/science.223.4640.1072

Esposito, L. W., Copley, M., Eckert, R., Gates, L., Stewart, A. I. F., & Worden, H. (1988). Sulfur dioxide at the Venus cloud tops, 1978–1986. *Journal of Geophysical Research*, *93*(D5), 5267–5276. https://doi.org/10.1029/JD093iD05p05267

Fedorova, A., Marcq, E., Luginin, M., Korablev, O., Bertaux, J. L., & Montmessin, F. (2016). Variations of water vapor and cloud top altitude in the Venus' mesosphere from SPICAV/VEx observations. *Icarus*, *275*, 143–162. https://doi.org/10.1016/j.icarus.2016.04.010

Gao, P., Zhang, X., Crisp, D., Bardeen, C. G., & Yung, Y. L. (2014). Bimodal distribution of sulfuric acid aerosols in the upper haze of Venus. *Icarus*, *231*, 83–98. https://doi.org/10.1016/j.icarus.2013.10.013

Hansen, J. E., & Hovenier, J. W. (1974). Interpretation of the polarization of Venus. *Journal of the Atmospheric Sciences*, *31*(4), 1137–1160. https://doi.org/10.1175/1520-0469(1974)031<1137:IOTPOV>2.0.CO;2

Ignatiev, N. I., Moroz, V. I., Zasova, L. V., & Khatuntsev, I. V. (1999). Water vapour in the middle atmosphere of Venus: An improved treatment of the Venera 15 ir spectra. *Planetary and Space Science*, *47*(8–9), 1061–1075. https://doi.org/10.1016/S0032-0633(99)00030-6

Imamura, T., Ando, H., Tellmann, S., Pätzold, M., Häusler, B., Yamazaki, A., et al. (2017). Initial performance of the radio occultation experiment in the Venus orbiter mission Akatsuki. *Earth, Planets and Space*, *69*(1), 1–11. https://doi.org/10.1186/s40623-017-0722-3

Jessup, K. L., Marcq, E., Mills, F., Mahieux, A., Limaye, S., Wilson, C., et al. (2015). Coordinated hubble space telescope and Venus express observations of Venus' upper cloud deck. *Icarus*, *258*, 309–336. https://doi.org/10.1016/j.icarus.2015.05.027

Knollenberg, R. G., & Hunten, D. M. (1980). The microphysics of the clouds of Venus: Results of the Pioneer Venus particle size spectrometer experiment. *Journal of Geophysical Research*, *85*(A13), 8039–8058. https://doi.org/10.1029/JA085iA13p08039

Krasnopolsky, V. A. (2010). Spatially-resolved high-resolution spectroscopy of Venus 2. Variations of HDO, OCS, and SO_2 at the cloud tops. *Icarus*, *209*(2), 314–322. https://doi.org/10.1016/j.icarus.2010.05.008

Krasnopolsky, V. A. (2012). A photochemical model for the Venus atmosphere at 47–112 km. *Icarus*, *218*(1), 230–246. https://doi.org/10.1016/j.icarus.2011.11.012

Krasnopolsky, V. A. (2013). S_3 and S_4 abundances and improved chemical kinetic model for the lower atmosphere of Venus. *Icarus*, *225*(1), 570–580. https://doi.org/10.1016/j.icarus.2013.04.026

Krasnopolsky, V. A. (2015). Vertical profiles of H_2O, H_2SO_4, and sulfuric acid concentration at 45–75 km on Venus. *Icarus*, *252*, 327–333. https://doi.org/10.1016/j.icarus.2015.01.024

Krasnopolsky, V. A. (2018). Disulfur dioxide and its near-UV absorption in the photochemical model of Venus atmosphere. *Icarus*, *299*, 294–299. https://doi.org/10.1016/j.icarus.2017.08.013

Krasnopolsky, V. A., Belyaev, D. A., Gordon, I. E., Li, G., & Rothman, L. S. (2013). Observations of D/H ratios in H_2O, HCl, and HF on Venus and new DCl and DF line strengths. *Icarus*, *224*(1), 57–65. https://doi.org/10.1016/j.icarus.2013.02.010

Lefevre, M., Lebonnois, S., & Spiga, A. (2018). Three-dimensional turbulence-resolving modeling of the Venusian cloud layer and induced gravity waves: Inclusion of complete radiative transfer and wind shear. *Journal of Geophysical Research: Planets*, *123*, 2773–2789. https://doi.org/10.1029/2018JE005679

Lefevre, M., Spiga, A., & Lebonnois, S. (2020). Mesoscale modeling of Venus' bow-shape waves. *Icarus*, *335*, 113376. https://doi.org/10.1016/j.icarus.2019.07.010

Limaye, S. S., Grassi, D., Mahieux, A., Migliorini, A., Tellmann, S., & Titov, D. (2018). Venus atmospheric thermal structure and radiative balance. *Space Science Reviews*, *214*(5), 102. https://doi.org/10.1007/s11214-018-0525-2

Marcq, E., Baggio, L., Lefèvre, F., Stolzenbach, A., Montmessin, F., Belyaev, D., et al. (2019). Discovery of cloud top ozone on Venus. *Icarus*, *319*, 491–498. https://doi.org/10.1016/j.icarus.2018.10.006

Marcq, E., Bertaux, J.-L., Montmessin, F., & Belyaev, D. (2013). Variations of sulphur dioxide at the cloud top of Venus's dynamic atmosphere. *Nature Geoscience*, *6*(1), 25–28. https://doi.org/10.1038/ngeo1650

Marcq, E., Lea Jessup, K., Baggio, L., Encrenaz, T., Joo Lee, Y., Montmessin, F., et al. (2019). Climatology of SO_2 and UV absorber at Venus' cloud top from SPICAV-UV nadir dataset. *Icarus*, *335*, 113368. https://doi.org/10.1016/j.icarus.2019.07.002

Mills, F. P. (1998). *I. Observations and photochemical modeling of the Venus middle atmosphere. II. Thermal infrared spectroscopy of Europa and Callisto* (Phd, California Institute of Technology). Retrieved from http://doi.org/10.7907/NWPG-E852

Na, C. Y., Esposito, L. W., & Skinner, T. E. (1990). International ultraviolet explorer observation of Venus SO_2 and SO. *Journal of Geophysical Research*, *95*(D6), 7485–7491. https://doi.org/10.1029/JD095iD06p07485

Parkinson, C. D., Gao, P., Esposito, L., Yung, Y., Bougher, S., & Hirtzig, M. (2015). Photochemical control of the distribution of Venusian water. *Planetary and Space Science*, *113-114*, 226–236. https://doi.org/10.1016/j.pss.2015.02.015

Sandor, B. J., & Clancy, R. T. (2005). Water vapor variations in the Venus mesosphere from microwave spectra. *Icarus*, *177*(1), 129–143. https://doi.org/10.1016/j.icarus.2005.03.020

Sandor, B. J., Clancy, R. T., & Moriarty-Schieven, G. (2012). Upper limits for H_2SO_4 in the mesosphere of Venus. *Icarus*, *217*(2), 839–844. https://doi.org/10.1016/j.icarus.2011.03.032

Sandor, B. J., Todd Clancy, R., Moriarty-Schieven, G., & Mills, F. P. (2010). Sulfur chemistry in the Venus mesosphere from SO_2 and SO microwave spectra. *Icarus*, *208*(1), 49–60. https://doi.org/10.1016/j.icarus.2010.02.013

Tellmann, S., Pätzold, M., Häusler, B., Bird, M. K., & Tyler, G. L. (2009). Structure of the Venus neutral atmosphere as observed by the Radio Science experiment VeRa on Venus Express. *Journal of Geophysical Research*, *114*, E00B36. https://doi.org/10.1029/2008JE003204

Vandaele, A. C., Korablev, O., Belyaev, D., Chamberlain, S., Evdokimova, D., Encrenaz, T., et al. (2017). Sulfur dioxide in the Venus atmosphere: II. Spatial and temporal variability. *Icarus*, *295*, 1–15. https://doi.org/10.1016/j.icarus.2017.05.001

Von Zahn, U., Krankowsky, D., Mauersberger, K., Nier, A. O., & Hunten, D. M. (1979). Venus thermosphere: In situ composition measurements, the temperature profile, and the homopause altitude. *Science*, *203*(4382), 768–770. https://doi.org/10.1126/science.203.4382.768

Woo, R., & Ishimaru, A. (1981). Eddy diffusion coefficient for the atmosphere of Venus from radio scintillation measurements. *Nature*, *289*(5796), 383–384. https://doi.org/10.1038/289383a0

Young, A. T. (1973). Are the clouds of Venus sulfuric acid? *Icarus*, *18*(4), 564–582. https://doi.org/10.1016/0019-1035(73)90059-6

Yung, Y. L., & DeMore, W. B. (1982). Photochemistry of the stratosphere of Venus: Implications for atmospheric evolution. *Icarus*, *51*(2), 199–247. https://doi.org/10.1016/0019-1035(82)90080-X

Zhang, X., Liang, M. C., Mills, F. P., Belyaev, D. A., & Yung, Y. L. (2012). Sulfur chemistry in the middle atmosphere of Venus. *Icarus*, *217*(2), 714–739. https://doi.org/10.1016/j.icarus.2011.06.016

Zhang, X., Liang, M. C., Montmessin, F., Bertaux, J. L., Parkinson, C., & Yung, Y. L. (2010). Photolysis of sulphuric acid as the source of sulphur oxides in the mesosphere of Venus. *Nature Geoscience*, *3*(12), 834–837. https://doi.org/10.1038/ngeo989

Zhang, X., Shia, R.-L., & Yung, Y. L. (2013). Jovian stratosphere as a chemical transport system: Benchmark analytical solutions. *The Astrophysical Journal*, *767*(2), 172. https://doi.org/10.1088/0004-637X/767/2/172